



A phase field study of the thermal migration of gas bubbles in UO_2 nuclear fuel under temperature gradient

Yafeng Wang^{a,b}, Zhihua Xiao^{a,b}, Shenyang Hu^c, Yulan Li^c, San-Qiang Shi^{a,b,*}

^a The Hong Kong Polytechnic University Shenzhen Research Institute, Shenzhen, China

^b Department of Mechanical Engineering, the Hong Kong Polytechnic University, Hung Hom, Kowloon, Hong Kong SAR

^c Pacific Northwest National Laboratory, 902 Battelle Blvd., Richland, WA 99352, USA

ARTICLE INFO

Keywords:

Gas bubble migration
Quantitative phase-field modeling
Temperature gradient

ABSTRACT

Phase field models are developed to study the gas bubble migration in uranium dioxide nuclear fuel in which a large temperature gradient exists during the operation. In this work, thermal diffusion mechanism for nanosized gas bubbles and vapor transport process for micron-sized gas bubbles are considered, respectively. In both cases, gas bubbles migrate to the high-temperature area. Due to the velocity difference between leading and trailing edges of the gas bubbles, nanosized gas bubbles are elongated along the temperature gradient direction when thermal diffusion is dominated. Micron-sized gas bubbles are either compressed along temperature gradient direction to form lenticular shape bubbles or elongated along temperature gradient direction, depending on the location of the gas bubbles within the fuel pellet. Initial gas bubble radius has no significant effect on the gas bubble migration velocity for both thermal diffusion and vapor transport mechanisms. We notice that the shape change of the gas bubble due to vapor transport mechanism has no significant effect on the migration velocity. Furthermore, the center cavity formation is also captured by our model which is due to the migration and accumulation of lenticular gas bubbles at the center of the fuel pellet. The modeling results compare well with experimental observations and theoretical analysis in the literature.

1. Introduction

UO_2 fuels are widely used in current nuclear power reactors and undergo extremely complex microstructure evolution during the operation [1,2]. Gaseous species (Xe, Kr) and vacancies are generated due to fission reactions and radiation damage, these gas atoms with extremely low solubility in the nuclear fuel tend to either combine with vacancies and then precipitate into bubbles or release to the free volume in UO_2 fuel pellets [3–7]. Owing to the continuous generation of fission gas bubbles and recrystallization in the UO_2 fuel, the thermal conductivity becomes non-uniform and changes with time [8–10], therefore, the temperature distribution becomes inhomogeneous, with a large thermal gradient formed from the center to the outer surface of the UO_2 fuel pellet [11,12]. Experimental results [13] confirmed that large temperature gradient and high level power could cause the migration and morphology change of gas bubbles and formation of a cavity in the center of the UO_2 fuel pellet which then behaves as a path for gas release. The migration and redistribution of gas bubbles lead to the formation of large columnar grains with inward orientation in the UO_2 fuel pellet [14]. The performance and lifespan of the UO_2 fuel

pellets are strongly dependent on the microstructure evolution especially the behavior of gas bubbles. Therefore, efficient utilization of UO_2 fuel requires a better understanding of the gas bubble evolution mechanisms.

Gas bubble migration mechanisms have been studied both through analysis [15,16] and experiments [17–19] for decades. The thermal diffusion mechanism was first used to explain the gas bubble migration. Because of thermal diffusion or so-called Soret effect [20], both heat flow and mass flux can be driven by the temperature gradient. A new migration mechanism was proposed when the movement of helium bubbles was studied in metals. Barns and Mazey [21] first suggested that the transport of matrix atoms via the vapor phase from the leading to the trailing edge of the gas bubble would contribute to the migration of gas bubble. Then, Speight [22] derived vapor transport velocity for gas bubbles due to the large temperature gradient in UO_2 fuel pellets. This mechanism is illustrated in Fig. 1, the up figure is an assumed cubic gas bubble, the bottom figure is a simple temperature profile which includes gas bubble and UO_2 matrix. The red dotted line represents the unperturbed temperature distribution in the matrix which the temperature decreases along positive x direction, and the blue line

* Corresponding author.

E-mail address: san.qiang.shi@polyu.edu.hk (S.-Q. Shi).

<https://doi.org/10.1016/j.commatsci.2020.109817>

Received 9 April 2020; Received in revised form 19 May 2020; Accepted 21 May 2020

Available online 29 May 2020

0927-0256/ © 2020 The Authors. Published by Elsevier B.V. This is an open access article under the CC BY-NC-ND license (<http://creativecommons.org/licenses/by-nc-nd/4.0/>).

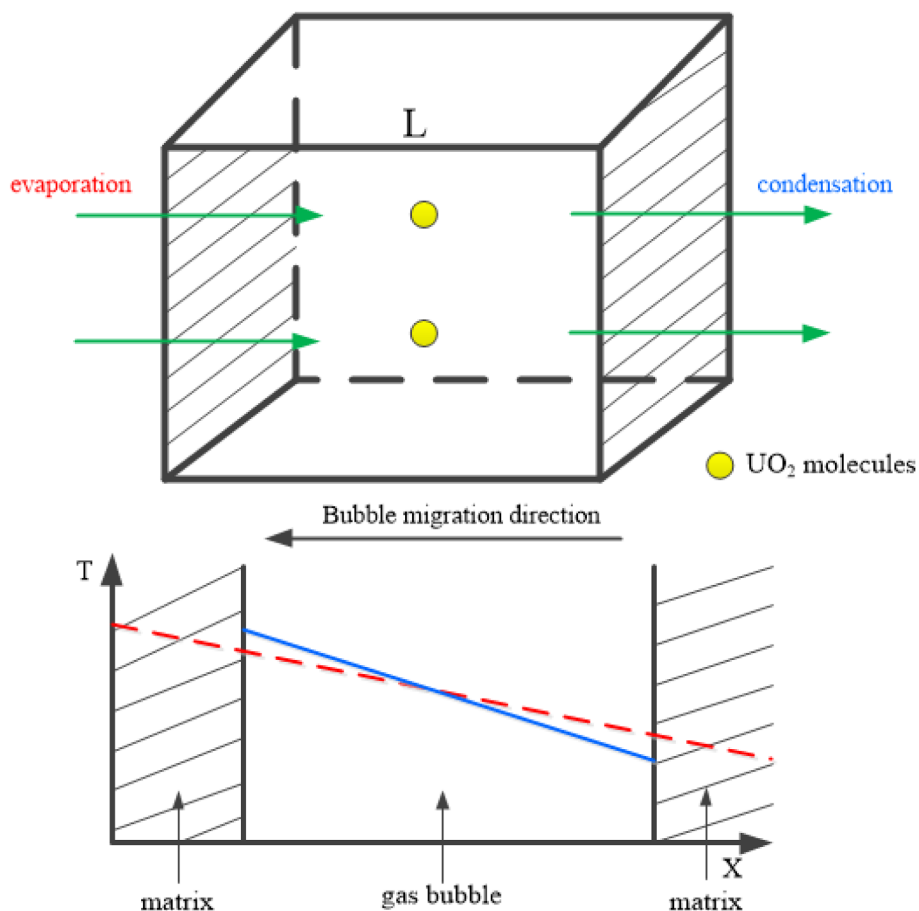


Fig. 1. Illustration of vapor transport mechanisms. The blue line is the real temperature distribution in the gas bubble, the red dot line is the unperturbed temperature distribution in matrix. (For interpretation of the references to colour in this figure legend, the reader is referred to the web version of this article.)

is the real temperature distribution in the gas bubble, which a larger temperature gradient is expected in the gas bubble. Due to the vapor pressure gradient caused by large temperature gradient, the UO_2 fuel evaporates at the hot side (left hand side in Fig. 1) of the gas bubble and then travels through the interior of the gas bubble and condensates at the cold side (right hand side in Fig. 1) of the gas bubble, at the same time the gas bubble moves to the left side where the temperature is higher. However, from the experimental results, one can not tell the precise migration mechanisms of the gas bubbles. Experiments showed some characteristics during the gas bubble migration process such as shape-change [19], small gas bubbles were emitted from micron-sized gas bubbles along the migration path [23], and formation of a cavity in the center of the UO_2 fuel pellet when the fuel undergoes high burnup [13].

In the recent years, with the development of high performance computers, numerical methods such as Potts Monte Carlo [24], molecular dynamics [25], phase-field method [26–29] and engineering-scale finite element simulations [30] have been applied to study the void migration process. As a mesoscale simulation approach, phase-field method is successfully used in studying the microstructure evolution in UO_2 fuel pellets [31–33]. Vance [27] and Zhang [26] considered the void migration by adding a flux term which is dependent on the temperature and temperature gradient in the diffusion equations. Zhang

[26] successfully coupled thermal conduction with phase field model, but failed to choose the right migration mechanism for void with a radius of $10\ \mu\text{m}$ and did not capture the void shape change during the migration. Vance [27] found the shape change of voids during the migration, however the voids had unrealistic size (radius of $15\ \mu\text{m}$) which are unusual in real UO_2 fuel pellets. Hu and Li [28,29] implemented the thermal diffusion mechanism by using a temperature dependent free energy function, however, their models did not capture the shape change of voids during migration which was observed in the experiments and analytical studies. In addition, the above phase field models only considered voids without gas atoms, and can only handle very high vacancy concentration in the order of 10^{-1} to 10^{-3} , which is also unrealistic in real UO_2 fuel pellets.

In this report, we propose two phase field models which could incorporate with thermal diffusion and vapor transport mechanisms, respectively, to simulate the migration process of gas bubbles with different sizes from several nanometers to several microns. A more physics-based free energy functional with realistic vacancy and gas atom concentrations in the fuel material is used. These models successfully capture the gas bubble shape-change during migration and center cavity formation process. Thermal diffusion mechanism is considered for gas bubbles in nanometer size, while the vapor transport mechanism is applied for gas bubbles in a size of a few micrometers. In

both cases, gas bubbles are found migrating up the temperature gradient.

2. Model description

2.1. Gas bubble migration models

Both temperature and concentration gradient can be the driving force which lead to the movements of gas bubbles. Mass flux can be caused by temperature gradient even when there is no concentration gradient, and the mass flux can cause heat flux at the same time. Due to the temperature gradient in the UO₂ fuel pellet, gas bubbles have a preferential motion direction related to the direction and magnitude of the heat transport. Speight [22] suggested that the mechanisms of gas bubble migration due to the temperature gradient are dependent on the gas bubble radius. For example, at 2000 K, thermal diffusion is the main mechanism when the bubble size is below a critical radius of 1 μm, otherwise, vapor transport plays the dominant role for larger gas bubbles. In this study, we consider thermal diffusion and vapor transport mechanisms for gas bubbles with different radii.

For the thermal diffusion process, according to the assumption of irreversible thermodynamics and Onsager relations, Olander [34] derived the force acting on the gas bubble by calculating the heat flux and mass flux caused by the large temperature gradient in the UO₂ nuclear fuel and gave the following expression:

$$F_b = \frac{4\pi R^3 Q_v^*}{3V_a T} \left(\frac{dT}{dx} \right)_b \quad (1)$$

where F_b is the force acting on the gas bubble, R is the radius of the gas bubble, V_a is volume transferred per atom, Q_v^* is the heat of transport and the subscript b means the temperature gradient in the gas bubble, T is the absolute temperature. Due to the low thermal conductivity of gas, we have $(dT/dx)_b > (dT/dx)_m$ where subscript m means the temperature gradient in the matrix. Here we assume $(dT/dx)_b = 2.2(dT/dx)_m$ [26] for gas bubbles containing Xe gas atoms. Then according to Nichols's derivation [35], the velocity due to the thermal diffusion may be given as:

$$V_b = M_b F_b \quad (2)$$

where $M_b = 3VD_b/(4\pi R^3 k_B T)$ is gas bubble mobility, D_b is the diffusivity. Here, we assume this diffusivity equals the diffusivity of vacancy [36]. According to the Eq. (1), if the heat of transport (Q_v^*) has positive value, the mass flux will flow down the temperature gradient, and the heat will flow from hot area to cold area. In this circumstance, the force on the gas bubbles is in the opposite direction to the temperature gradient, therefore gas bubbles will migrate up the temperature gradient, moving to high temperature area (the center of the UO₂ fuel pellet).

Gas bubble migration velocity due to vapor transport was first derived by Speight [22], then Sens [23] modified Speight's equation. In Speight's derivation, the internal pressure of gas bubbles is balanced by the surface tension. Under this circumstance, the migration velocity is linearly dependent on gas bubble radius:

$$V_b = Ar \frac{dT}{dx} \quad (3)$$

where r is the gas bubble radius, A is a prefactor. According to Speight's derivation, it was assumed that the internal pressure is always balanced by the surface tension which requires the gas bubble keeping the spherical shape during the migration, whereas the experimental

results showed that gas bubbles changed morphology during the migration. Therefore, Sens's derivation begun with the assumption that the internal pressure of the gas bubble is independent of surface tension and gas bubble radius, and only determined by the local temperature in the UO₂ fuel pellet. Sens gave an expression for the vapor transport velocity for gas bubbles as a function of temperature and temperature gradient:

$$V_b = J_A \Omega = \alpha \left(\sum_{i=0}^3 a_i T^i \right) T^{-5/2} \Delta H p_0 \exp\left(-\frac{\Delta H}{RT}\right) \left(\frac{dT}{dx} \right)_m \quad (4)$$

where J_A is the UO₂ molecule flux, Ω is the volume of a UO₂ molecule, α and a_i are prefactors, ΔH is the enthalpy of vaporization of UO₂, p_0 is the pressure prefactor which has something to do with the pressure and pressure gradient, and these values can be obtained from [23]. The vapor pressure in UO₂ fuel pellet equals to $p_0 \exp(-\Delta H/RT)$.

2.2. Phase-field model for gas bubble migration

KKS model [37] is used here to study the movement of nanosized gas bubbles. The total free energy of the system with vacancies, gas atoms and gas bubbles is given as:

$$F = N \int_V (1 - h(\eta)) f^m(c_v^m, c_g^m) + h(\eta) f^b(c_v^b, c_g^b) + w g(\eta) + \frac{\kappa^2}{2} |\nabla \eta|^2 dV \quad (5)$$

where η is the order parameter, which equals to zero inside the UO₂ matrix and unity inside gas bubbles, $h(\eta) = \eta^3(6\eta^2 - 15\eta + 10)$ is the interpolation function which describes the volume fraction of the gas bubble phase, and changes smoothly from $h(0) = 0$ to $h(1) = 1$ in the interface between the UO₂ matrix and gas bubbles. $g(\eta) = \eta^2(\eta - 1)^2$ is a double well potential which has two local minima (i.e. $\eta = 0$ in the matrix phase and $\eta = 1$ in gas bubble phase), and it only contributes to the chemical free energy at the interface ($0 < \eta < 1$). $w = 3\alpha_s \gamma_s / \lambda$ is the height of the double well potential. α_s is a constant which is dependent on the definition of the interface thickness, and it is set to 2.2 in the simulation [37]. 2λ is the interface thickness. $\gamma_s = 0.85 - 1.4 \times 10^{-4}(T - 273) \text{ J/m}^2$ is the surface tension [38], T is the absolute temperature. $\kappa = \sqrt{6\gamma_s \lambda / \alpha_s}$ is the gradient coefficient. N is the number of lattice sites per unit volume of UO₂. V is the total volume of the system.

f^m and f^b are chemical free energy density of UO₂ matrix and gas bubble, respectively. Since the nanosized gas bubbles are in solid or liquid state [39], the regular solution model is used in the configuration of the system free energy. Chemical free energy density of the matrix and gas bubble are given below, the detailed derivation can be found in Appendix A.

$$f^m(c_v^m, c_g^m) = k_B T \left[c_v^m \ln \frac{c_v^m}{c_{ve}^m} + c_g^m \ln \frac{c_g^m}{c_{ge}^m} + (1 - c_v^m - c_g^m) \ln \frac{1 - c_v^m - c_g^m}{1 - c_{ve}^m - c_{ge}^m} \right] \quad (6a)$$

$$f^b(c_v^b, c_g^b) = k_B T \left[c_v^b \ln \frac{c_v^b}{c_{ve}^b} + (1 - c_v^b) \ln \frac{1 - c_v^b}{1 - c_{ve}^b} + c_g^b \ln \frac{c_g^b}{c_{ge}^b} + (c_{gm} - c_g^b) \ln \frac{c_{gm} - c_g^b}{c_{gm} - c_{ge}^b} \right] \quad (6b)$$

where k_B is the Boltzmann constant. c_v^m and c_g^m are the vacancy concentration and gas atom concentration in the matrix, respectively. $c_{ve}^m = \exp(-E_v^f/k_B T)$ and $c_{ge}^m = \exp(-E_g^f/k_B T)$ are the thermodynamic equilibrium vacancy concentration and gas atom concentration in the matrix, respectively. E_v^f and E_g^f are the vacancy and gas atom formation

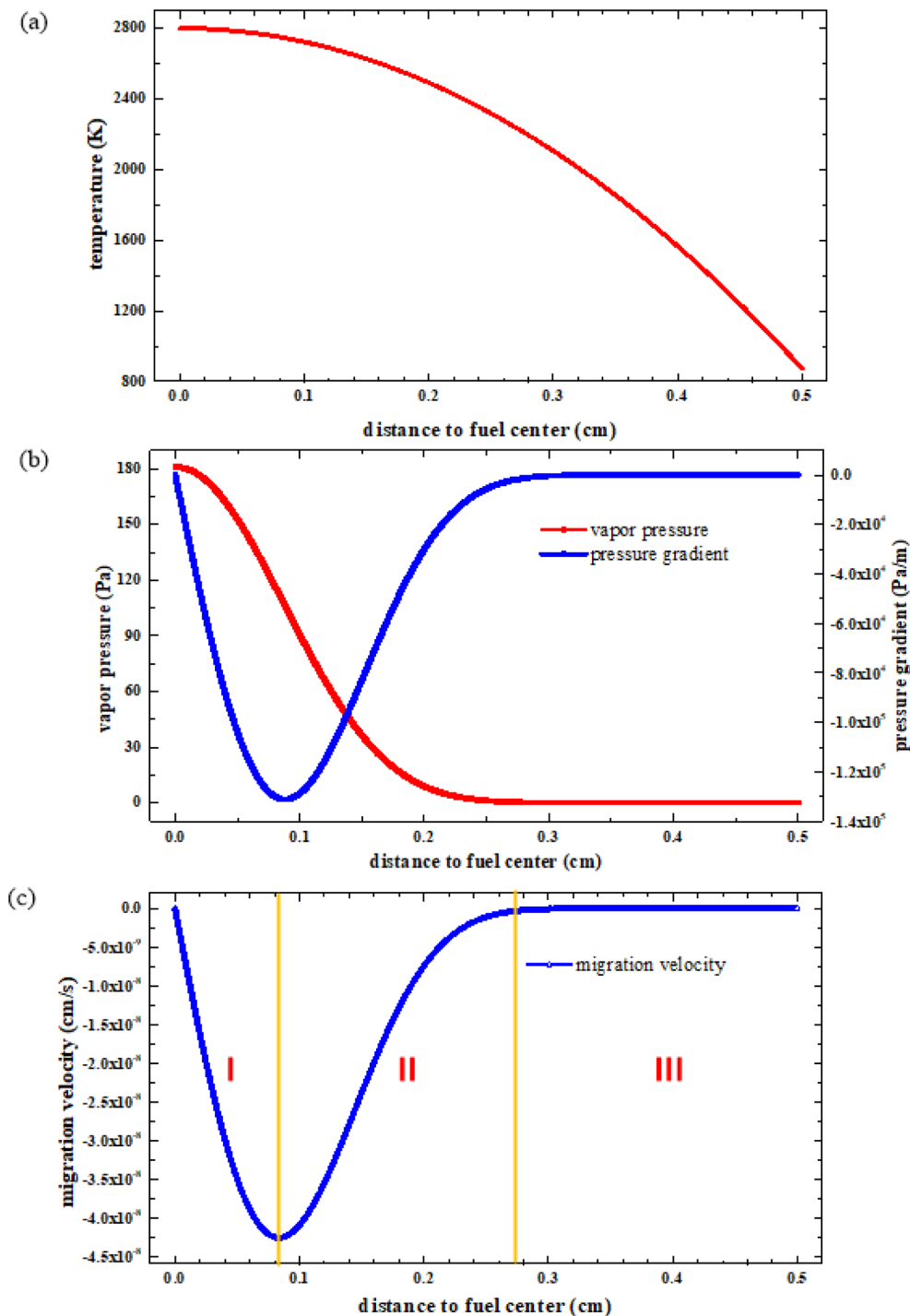


Fig. 2. (a) Assumed parabolic temperature file (top) in the radial direction of the fuel pellet, (b) vapor pressure (red line) and vapor pressure gradient (blue line) in the UO_2 matrix, (c) the vapor transport velocity profile according to Sens's derivation [23]. The negative vapor transport velocity means the gas bubble will move from the outer surface to the center of a fuel pellet. (For interpretation of the references to colour in this figure legend, the reader is referred to the web version of this article.)

energy, respectively. c_{ve}^b and c_{ge}^b are the thermodynamic equilibrium concentrations of vacancy and gas atom in the bubble, respectively. c_{ve}^b should be a value very close to 1 (100%), physically. It is set to 0.99 in this model. This is due to the fact that nano-sized gas bubbles are in solid or liquid state [39] and the UO_2 particle is considered as one unit

lattice point in this work. Some UO_2 particles may be inside the bubbles mixed with gas atoms due to irradiation cascade or diffusion. $c_{ge}^b = \frac{\Omega}{rk_B T / 2\gamma_s + b}$ is derived based on Van der Waals equation of state, the detailed derivation can be found in Appendix B. $c_{gm} = \Omega/b$ is the maximum gas atom concentration in the gas bubble. For Xe gas atoms,

$b = 0.085 \text{ nm}^3/\text{atom}$, $\Omega = 0.041 \text{ nm}^3/\text{molecule}$ for a UO_2 molecule.

Following KKS model, the concentration of vacancy and gas atoms are written as:

$$c_v = (1 - h(\eta))c_v^m + h(\eta)c_v^b \quad (7a)$$

$$c_g = (1 - h(\eta))c_g^m + h(\eta)c_g^b \quad (7b)$$

The Cahn-Hilliard diffusion equations with thermal diffusion terms [40,41] for vacancies and gas atoms under temperature gradient are:

$$\frac{\partial c_v}{\partial t} = \nabla \cdot \left(M_v \nabla \frac{\delta F}{\delta c_v} + \frac{M_v c_v Q^*}{T} \nabla T \right) \quad (8a)$$

$$\frac{\partial c_g}{\partial t} = \nabla \cdot \left(M_g \nabla \frac{\delta F}{\delta c_g} + \frac{M_g c_g Q^*}{T} \nabla T \right) \quad (8b)$$

where, M_v and M_g are the mobilities of vacancy and gas atom, respectively, and have the form $M_v = D_v/k_B T$ and $M_g = D_g/k_B T$, respectively, Q^* is the heat transport and $Q^* = Q_v^*$. Here, D_v and D_g are the diffusion coefficients of vacancy and Xe gas atoms, respectively. $D_v = D_{v0} \exp(-E_v^m/k_B T)$ and $D_g = D_{g0} \exp(-E_g^m/k_B T)$, where E_v^m and E_g^m are the migration energy of vacancy and Xe gas atom, respectively. D_{v0} and D_{g0} are the prefactors of vacancy and Xe gas atom diffusion coefficients, respectively. The second term in right hand side of Eq.(8a) and (8b) are the thermal diffusion terms due to the temperature gradient. The Allen-Cahn equation [42] for gas bubble evolution is written as follows:

$$\frac{\partial \eta}{\partial t} = -L \frac{\delta F}{\delta \eta} \quad (9)$$

where L is the interface mobility.

For micron-sized gas bubbles, since the bubbles are in gas state, a simple chemical free energy density is assumed:

$$f(c_v, c_g) = a(c_v - c_{ve}^m)^2(c_g - c_{ge}^b)^2 + b(c_v - c_{ve}^b)^2(c_g - c_{ge}^m)^2 \quad (10)$$

where a and b are pre-factors. To simplify the simulation, a and b are assumed to be 1. Then the total free energy is written as:

$$F = \int_V \left[f(c_v, c_g) + \frac{\kappa_{c_g}}{2} (\nabla c_g)^2 + \frac{\kappa_{c_v}}{2} (\nabla c_v)^2 \right] dV \quad (11)$$

where κ_{c_g} and κ_{c_v} are gradient coefficients of gas atom and vacancy, respectively. Then Cahn-Hilliard diffusion equations with advection terms [27] are used to solve for the dynamic evolution of micro-sized gas bubbles:

$$\frac{\partial c_v}{\partial t} = \nabla \cdot \left(M_v \nabla \frac{\delta F}{\delta c_v} \right) - \nabla \cdot (V_b c_v) \quad (12a)$$

$$\frac{\partial c_g}{\partial t} = \nabla \cdot \left(M_g \nabla \frac{\delta F}{\delta c_g} \right) - \nabla \cdot (V_b c_g) \quad (12b)$$

A few assumptions are made in deriving the above models for nano and micro-sized bubbles. First, we did not consider the elastic strain energy in the system, and the system is under stress-free state. The influence of elastic strain energy on gas bubbles evolution can be found from our another work, which is only effective in very short distance. Second, there are no newly generated vacancies or gas atoms in the UO_2 matrix, which is corresponding to the out of pile thermal annealing process. The effect of irradiation on gas bubble migration cannot be found in literature, however the effects of irradiation and defect

Table 1
Material parameters used in the simulation.

Parameter	Value	Ref
E_v^f	3.27 eV	[46]
E_g^f	3.27 eV	
E_v^m	2.4 eV	[47]
E_g^m	2.4 eV	[47]
D_{v0}	2.0×10^{-7}	[47]
D_{g0}	5.0×10^{-5}	[47]
Q_v^*	4.0 eV	[26]
ΔH	$6.35 \times 10^5 \text{ J/mol}$	[23]
$\ln p_0$	35.8130	[23]

generation on voids and gas bubbles growth have been studied elsewhere [43,44].

The Eq.(8a), (8b), (9), (12a) and (12b) are solved by finite difference method. Two-dimensional simulations are performed. For thermal diffusion process, our focus is on nano-sized gas bubbles. In this case, a uniform rectilinear grid with 40×70 nodes is used for discretization, the grid size is $\Delta x = \Delta y = 5 \text{ nm}$, therefore the simulation domain is $200 \text{ nm} \times 350 \text{ nm}$. Three constant temperature gradients, $\nabla T = 1 \text{ K}/\mu\text{m}$, $\nabla T = 0.8 \text{ K}/\mu\text{m}$ and $\nabla T = 0.4 \text{ K}/\mu\text{m}$ are applied respectively in the y -direction of simulation domain which corresponds to the radial direction in the fuel pellet. The temperature is set as 2000 K at the bottom ($y = 0$) of the simulation domain and increases from the bottom edge. Time step is set as $\Delta t = 1.0 \times 10^{-6} \text{ s}$. For vapor transport process, the concerned gas bubble radius is in the order of microns. Therefore, the grid size is set as $\Delta x = \Delta y = 0.1 \mu\text{m}$, and simulation domains are $10 \mu\text{m} \times 100 \mu\text{m}$ and $51.2 \mu\text{m} \times 51.2 \mu\text{m}$, respectively. In this case, a parabolic temperature profile [27,45] is used with the fuel pellet center temperature of 2800 K, decreasing from the fuel center to the outer surface of the fuel pellet, according to the distribution of temperature in UO_2 (Fig. 2 (a)), the vapor pressure [23] is also given in Fig. 2 (b). Vapor transport velocity profile is shown in Fig. 2 (c), the negative sign means that the gas bubble will migrate along the radial direction from the fuel outer surface to the fuel center. When comparing Fig. 2 (b) and Fig. 2 (c), the vapor transport velocity has the same tendency as vapor pressure gradient in the UO_2 matrix.

Parameters used in this study are listed in Table 1.

3. Results and discussion

Gas bubbles with different initial shapes (circular or ellipse shape) are implanted in the simulation domains. For the thermal diffusion process, the temperature is set as 2000 K at the bottom of the simulation domain and increases from the bottom to the top of the domain. Nano-sized gas bubbles are often found in circular shape in UO_2 nuclear fuel pellets, therefore a circular gas bubble has an initial radius of 25.0 nm and is located at $x = 20\Delta x$, $y = 10\Delta y$. Fig. 3 (contour of order parameter η) delineates successive snapshots of this single gas bubble as it migrates in the domain under a temperature gradient of 1 K/ μm . Typically, the temperature gradient in UO_2 fuel pellet is around 0.1–0.6 K/ μm . Oldfield used a laser image furnace to get a temperature gradient of 3.9 °C/ μm [13], and Whapham reported a temperature gradient of 10⁶ °C/cm by using Pulse-anneal technique to study the migration of fission-gas bubbles in irradiated UO_2 [48]. As expected, the gas bubble migrates toward the hot side of the simulation domain. It is noteworthy

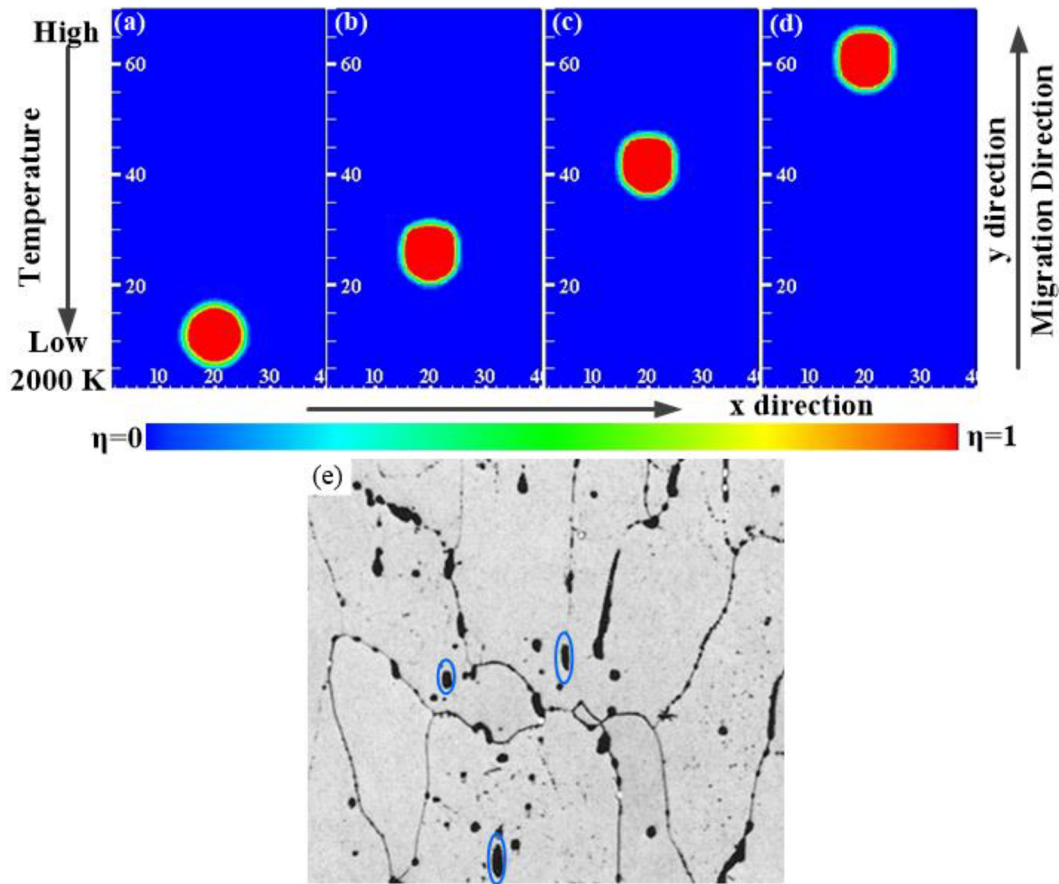


Fig. 3. Single gas bubble migration in the temperature gradient of 1 K/μm, the temperature decreases from the top to the bottom of the simulation domain, a), b), c), d) the location and shape of the gas bubble at 0 s, 20 s, 40 s and 65 s, respectively, (e) elongated gas bubbles marked with blue circles, and the bottom is toward the center of the fuel pellet [23]. (For interpretation of the references to colour in this figure legend, the reader is referred to the web version of this article.)

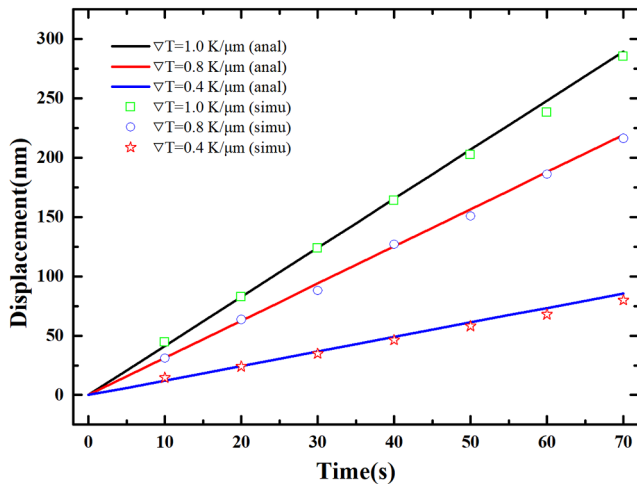


Fig. 4. Comparison of gas bubble migration displacement between phase field simulations and analysis solution of Eq.(2). Symbols and solid lines represent the simulation and analysis results, respectively.

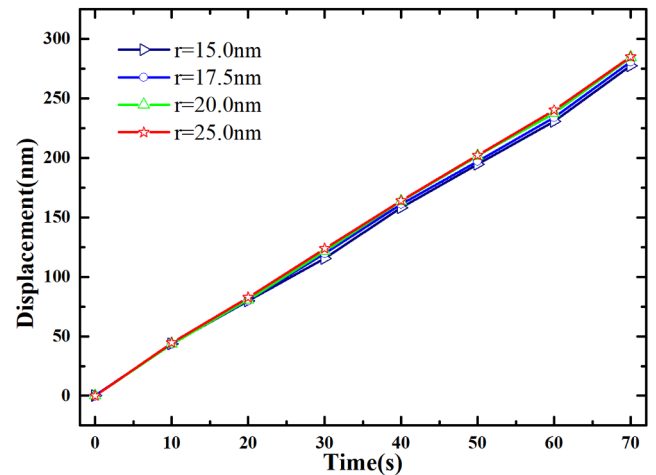


Fig. 5. Displacement of gas bubbles with different initial radii in the temperature gradient of 1 K/μm.

that this circular gas bubble is elongated in the y-direction and compressed in the x-direction, and the morphology changes from a circular to an ellipse shape which was also observed in experiments [23] in Fig. 3 (e) (bubbles are marked by blue circles). Fig. 3 (e) came from a used UO₂ fuel sample which underwent irradiation. The gas bubbles

were generated continually when it was under irradiation, and the newly generated gas bubbles are usually smaller and have a circular shape. Some bubbles generated earlier in the UO₂ fuel pellet (usually bigger in size) had migrated under the temperature gradient and changed shape. Fig. 3 (e) shows older bubbles with elongated shape and newly generated bubbles with circular shape at the same time in the sample. According to Eq.(2), the migration velocity depends on the gas

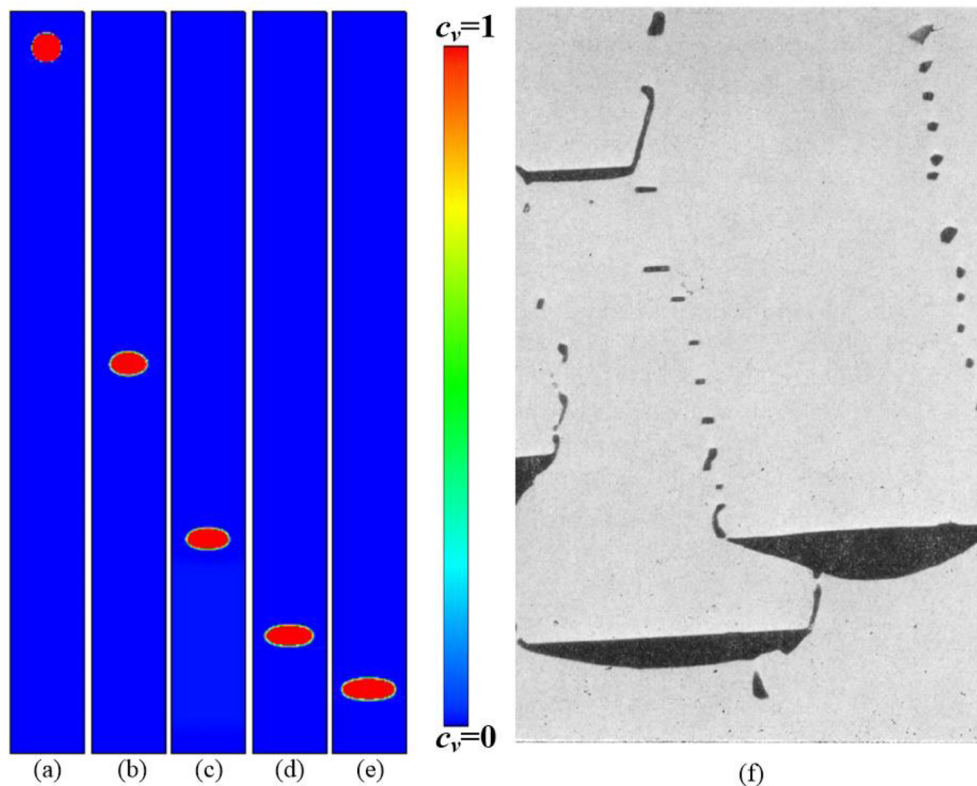


Fig. 6. Single gas bubble migration under the conditions given in the region I of Fig. 2 (c). (a) to (e) correspond to 0 h, 200 h, 400 h, 600 h and 800 h, respectively. The bottom of the domain corresponds to the center of the fuel pellet where the temperature reaches the maximum value. (f) Experimental observations of gas bubbles with lenticular shape moving towards the fuel center (at the bottom of the photo) where the temperature is the highest [23].

bubble mobility. The leading edge of the gas bubble is in the high-temperature side which has higher mobility than the trailing edge. As a consequence, this velocity difference causes the gas bubble morphology to change from circle to prolate shape. This gas bubble continues moving along the y -direction where the temperature is also increasing. However, the difference in velocity between the leading and trailing edges become smaller when the bubble is close to the center of the fuel pellet. Therefore, it is expected that the shape will change back from prolate shape to circular shape when the bubble reaches the center of the fuel pellet.

To make a quantitative comparison of phase field modeling with the analytical solution of Eq.(2), three different temperature gradients are applied respectively, and the displacements within 70 s at different temperature gradients are depicted in Fig. 4. As can be seen, the phase field modeling results agree well with analytical results. The out of pile thermal annealing experiments showed that nano-sized gas bubbles have migration velocity of 4 nm/s which agrees well with the simulation results when the temperature gradient is set as 1 K/ μm [49]. According to Eq.(2), the gas bubble migration velocity has nothing to do with the gas bubble radius. To confirm this analysis, gas bubbles with different initial radii are used in the simulation. Fig. 5 shows the displacements of single gas bubble with different initial radius changing from 15.0 nm to 25.0 nm. As being expected, there is only slight difference found in the displacements. The simulation results confirm the prediction of Eq.(2), and the gas bubble radius has no significant effect on the migration velocity. Similar conclusion was reached in Baker's experiments in which no clear dependence of nano-sized bubble migration velocity on bubble radius was found [49].

In the second case, the migration of micron-sized gas bubbles is

studied with only vapor transport mechanism. Here, the grid size is increased to $\Delta x = \Delta y = 100$ nm. In the first part, the simulation domain with 100×1000 nodes is generated and the y -direction corresponds to radial direction in the fuel pellet. First, gas bubbles near the UO_2 fuel pellet center are first studied which correspond to the part I in Fig. 2 (c). A single gas bubble with a radius of 2.0 μm is located at $x = 50\Delta x$ and $y = 950\Delta y$. Fig. 6 (contour of vacancy concentration) delineates successive snapshots of this single gas bubble as it migrates in the domain under the temperature and velocity profiles in Fig. 2. The simulation domain corresponds to the region adjacent to the center of the fuel, in which the bottom ($y = 0\Delta y$) of the domain is the fuel center and the top ($y = 1000\Delta y$) of the domain is 100 μm away from the fuel center, so that the temperature is increasing from the top to the bottom of the domain. Gas bubble positions within 800 h are shown in Fig. 6. The gas bubble migrates along the negative y -direction as expected and migration velocity is decreasing when the gas bubble getting near to the fuel center. More notably, the gas bubble is elongated perpendicular to the temperature gradient and finally changes to lenticular shape, which is consistent with experimental observations [13,23] shown in Fig. 6 (f). Besides, from Fig. 6 (c), (d) and (e), the gas bubble velocity slows down. This is because when the gas bubble gets closer to the fuel center, the temperature is increased, while the temperature gradient is decreased. Sens's model which considered the gas bubble shape change is proved to be true, while other previously suggested models did not consider shape change during the gas bubble migration [22]. In contrast to the velocity field in thermal diffusion case, the velocity of leading surface is less than the trailing surface, therefore the gas bubble is compressed in the y -direction (the direction of temperature gradient) and elongated perpendicular to the temperature gradient direction during the

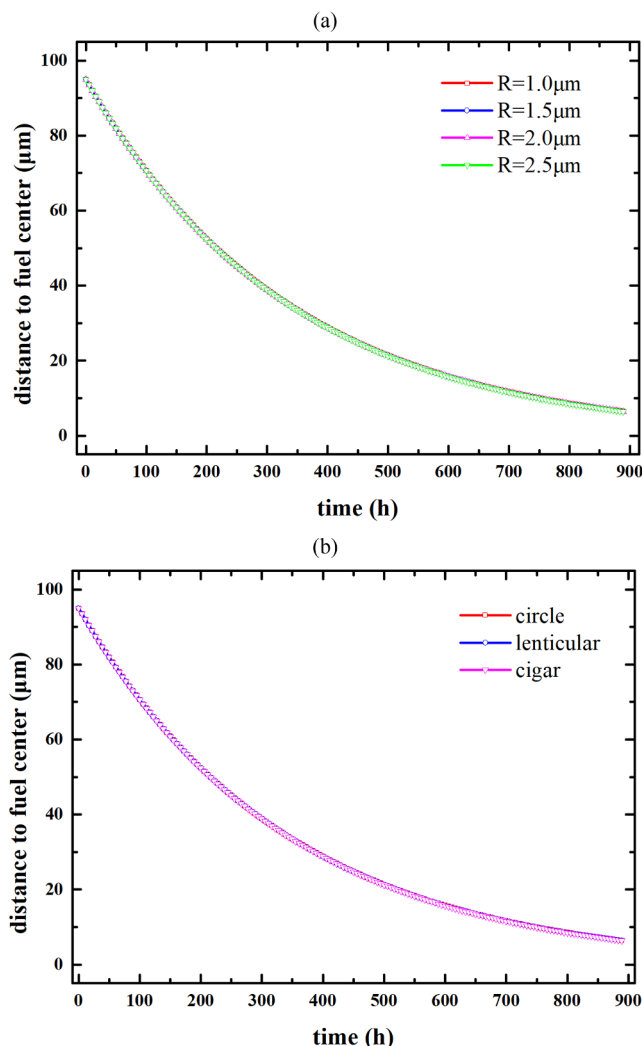


Fig. 7. (a) gas bubbles migration with different initial radii, (b) gas bubbles migration with different initial shapes.

migration. Sens modified Speight's model [22] by removing the gas bubble radius term from the velocity formulation with the assumption that the internal pressure of the gas bubble is independent of the gas bubble radius. To verify Sens's assumption that initial gas bubble radius has no effect on migration velocity, we only change the initial gas bubble radius and keep other parameters unchanged during the simulations, the result is showed in Fig. 7 (a). According to the simulation results, the initial gas bubble radius only has minor effects on migration velocity, and in this circumstance, Sens's model still works. The micro sized gas bubbles are found in many kinds of shapes in UO_2 fuel pellets. As a consequence, gas bubbles with different initial shapes are also studied, three different shapes, circular (with radius of $2\mu\text{m}$), lenticular (ellipse with $x = 2.5\mu\text{m}$, $y = 1.5\mu\text{m}$) and cigar (ellipse with $x = 1.5\mu\text{m}$, $y = 2.5\mu\text{m}$) shapes, respectively. The results are given in Fig. 7 (b). Gas bubbles with different initial shapes have the same velocity when migrate near the center of the fuel cell, this result is also confirmed by Nichols [45].

For gas bubbles which distribute in the region II in Fig. 2 (c), the same simulation domain size is used. The single gas bubble is located at $x = 50\Delta x$ and $y = 950\Delta y$. Fig. 8 (a) to (d) gives the positions of the gas bubble after 0, 200, 400 and 600 h, respectively. As the gas bubble getting near to the fuel center, the migration velocity increases which correspond to the conditions in Fig. 2 (c). The gas bubble is elongated when it migrates towards the fuel center, which is consistent to the experimental results given in Fig. 8 (e). From Fig. 8 (b), (c) and (d), the gas bubble is first elongated and then separates into two parts, which corresponds well to the gas bubbles marked by red circle in Fig. 8 (e). Due to the relatively higher velocity at the front edge and a lower velocity at the trailing edge, the initial spherical gas bubble is elongated along the direction of the temperature gradient, and at last the gas bubble breaks up into a line of small elongated gas bubbles, this is the phenomenon confirmed in Nichols's analysis [45].

The dramatic changes of gas bubble shape during the migration raises a question: Does the shape change of the gas bubble have any effect on the velocity during the migration? To answer this question, we calculate the velocities of the gas bubble at different positions in the simulation domain. To calculate the velocity of a bubble at a specific time step during migration, we need to determine the center position of the bubble at this moment. The center position of the bubble at a given moment is determined by adding all x -values and y -values of the points with the vacancy concentration larger than 0.6 (it means that point is within the bubble), and then averaging all the x -values and y -values respectively. With the positions of the gas bubble at different time steps, we can plot the velocity of the gas bubble versus position in Fig. 9. The red open circles are the simulation results as compared to the analytical result (blue line) from Eq.(4). Even though the gas bubble shape has dramatically changed, the migration velocity still matches the prediction with Eq.(4) very well. Nichols suggested [35] that the shape of the gas bubble has nothing to do with the migration velocity when vapor transport mechanism is considered. This opinion agrees well with Sens's analysis [23].

Another phenomenon in UO_2 fuel is the formation of a cavity in the center of the fuel pellet which could be the gas release path. This center cavity is believed to be the result of the aggregation of lenticular gas bubbles at high power level. In this case, we use a simulation domain with 512×512 nodes with a 2-D temperature profile (see Fig. 10 (e), temperature is high in the center and low on the surface). Four circular gas bubbles with the same initial radius are put into the simulation domain with center positions at $(x = 20.5\Delta x, y = 20.5\Delta y)$, $(x = 490.5\Delta x, y = 490.5\Delta y)$, $(x = 20.5\Delta x, y = 490.5\Delta y)$ and $(x = 490.5\Delta x, y = 20.5\Delta y)$, respectively. From Fig. 10 (a), (b) and (c), one can find that gas bubble shapes changed (compressed shape in radial direction). The four gas bubbles migrate along the radial direction towards to the center of the simulation domain. In Fig. 10 (c) and (d), they first contact with each other and eventually merge into one cavity in the center. An experimental observation of the center cavity formation is given in Fig. 10 (f), which acts as a gas release path for gas bubbles.

4. Conclusions

In summary, phase field models are developed to study the gas bubble migration under the temperature gradient in UO_2 nuclear fuel pellet, in which thermal diffusion mechanism for nano-sized gas bubbles and vapor transport process for micron-sized gas bubbles are

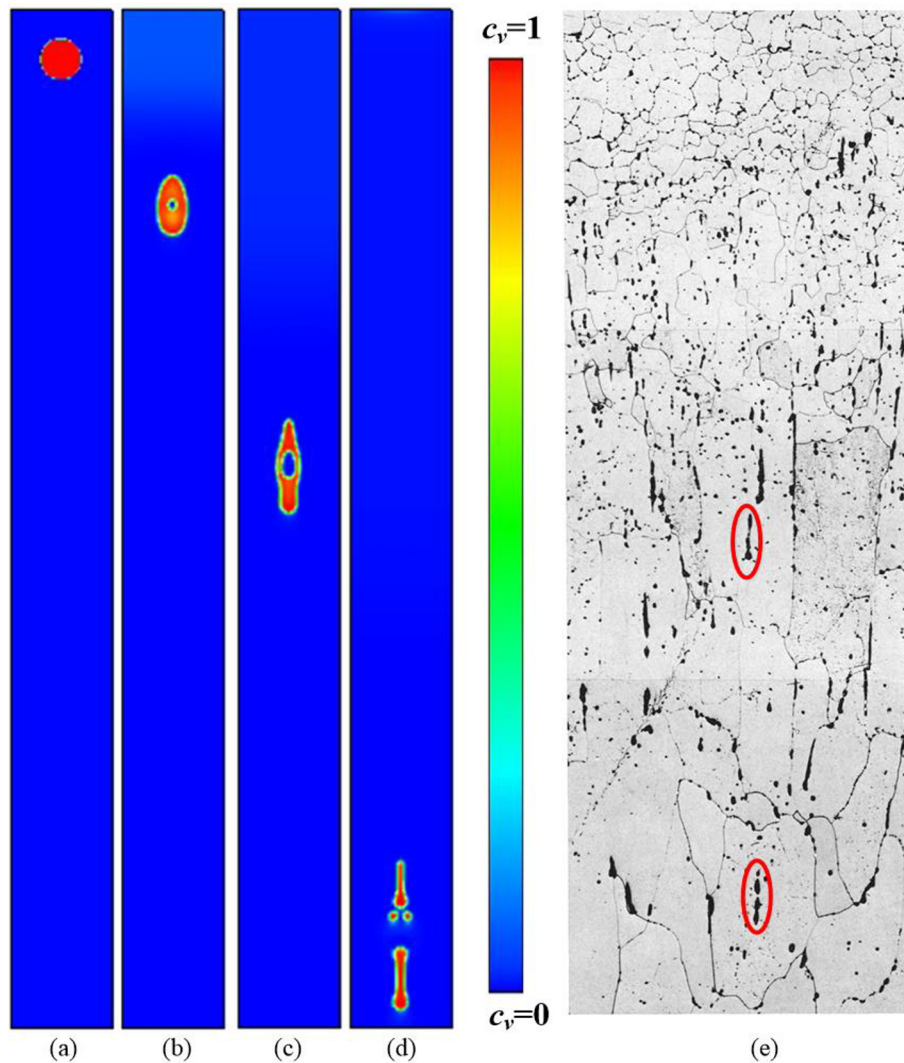


Fig. 8. Single gas bubble migration under the conditions by region II in Fig. 2 (c). (a) to (d) correspond to 0 h, 200 h, 400 h and 600 h, respectively, (e) Pores in region II in Fig. 2 (c), pointing towards the center of the fuel (bottom) [23].

considered. In both cases, gas bubbles migrate to the high-temperature area. Due to the velocity difference between leading and trailing edges of the gas bubbles, nano-sized gas bubbles are elongated along the temperature gradient direction when thermal diffusion is dominated. Micron-sized gas bubbles are either compressed along temperature gradient direction to form lenticular shape bubbles or elongated along temperature gradient direction, depending on the location of the gas bubbles within the fuel pellet. Initial gas bubble radius has no significant effect on the gas bubble migration velocity for both thermal diffusion and vapor transport mechanisms. We notice that the shape-change of the gas bubble due to vapor transport mechanism has no significant effect on the migration velocity. Furthermore, the center cavity formation is also captured by our model which is due to the

migration and accumulation of lenticular gas bubbles at the center of the fuel pellet. The above modeling results are consistent with experimental observations as well as theoretical analysis in the literature.

CRediT authorship contribution statement

Yafeng Wang: Investigation, Formal analysis, Writing - original draft. **Zhihua Xiao:** Validation. **Shenyang Hu:** Validation. **Yulan Li:** Validation. **San-Qiang Shi:** Writing - review & editing, Supervision.

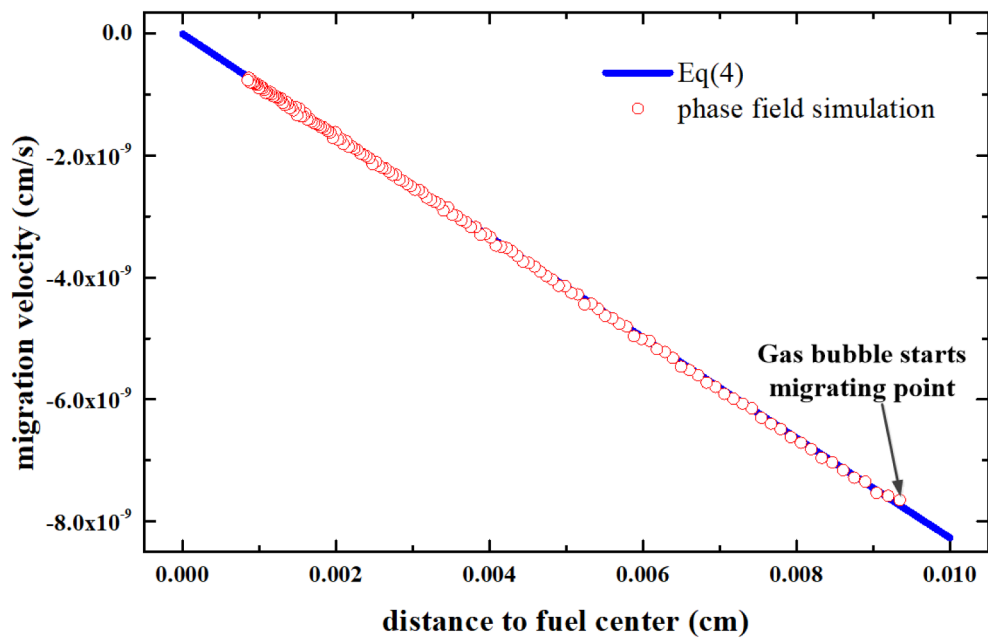


Fig. 9. Comparison of gas bubble migration velocity predicted by analytical model (blue line) with phase field simulation (red circles). (For interpretation of the references to colour in this figure legend, the reader is referred to the web version of this article.)

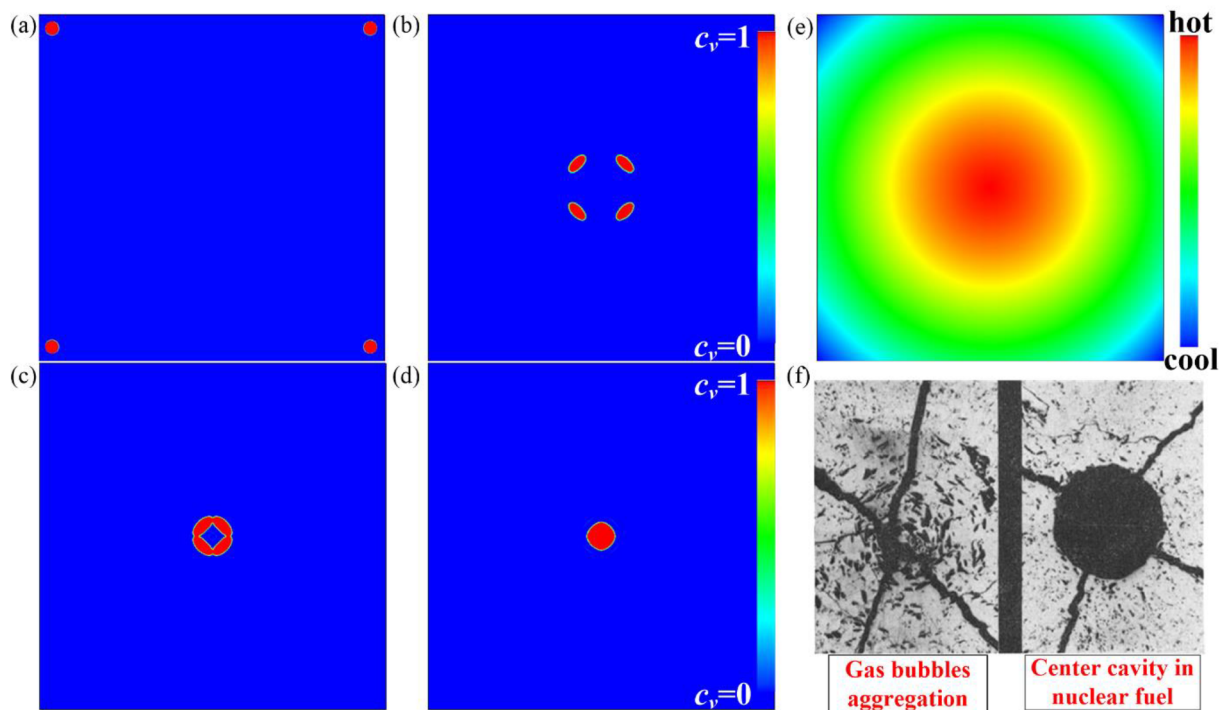


Fig. 10. Center cavity formation in the center of the simulation domain. (a), (b), (c) and (d) are the positions of gas bubbles at different times; (e) the 2-D temperature profile; (f) the high concentration of gas bubbles in the fuel center (left) and the formation of a center cavity at high level power (right) [23].

Declaration of Competing Interest

The authors declare that they have no known competing financial interests or personal relationships that could have appeared to influence the work reported in this paper.

Acknowledgements

This work was supported by grants from the National Natural Science Foundation of China (No. 51672232) and from the Research Grants Council of Hong Kong (PolyU 152636/16E).

Appendix A

Derivation of chemical free energy density of the matrix

Assume that UO_2 are crystals consisting of UO_2 particles. A vacancy is a lattice site at which the UO_2 particle is removed. Gas atoms occupy substitutional sites. There are n sites in total, which include $n-n_v-n_g$ lattice sites, n_v vacancy sites, and n_g sites occupied by gas atoms in the system. The total number of microstates in the matrix is

$$w^m = \frac{n!}{n_v!n_g!(1-n_v-n_g)!} \quad (\text{A1})$$

Then, the entropy is

$$\begin{aligned} s^m &= k_B \ln w^m = k_B \ln \frac{n!}{n_v!n_g!(1-n_v-n_g)!} \\ &\approx -nk_B [c_v^m \ln c_v^m + c_g^m \ln c_g^m + (1-c_v^m-c_g^m) \ln(1-c_v^m-c_g^m)] \end{aligned} \quad (\text{A2})$$

where $c_v^m = n_v/n$ and $c_g^m = n_g/n$, $n = 1/\Omega$, Ω the volume of a UO_2 particle.

The introduction of vacancies and gas atoms into the matrix changes the enthalpy of the system. Because the vacancy concentration and the gas atom concentration are very diluted in the matrix, the cross-interaction terms and the higher-order terms in enthalpy are omitted. Then, the enthalpy is

$$H^m = \Delta h_v^m n_v + \Delta h_g^m n_g + \Delta h_m^m n_m = n [\Delta h_v^m c_v^m + \Delta h_g^m c_g^m + \Delta h_m^m (1-c_v^m-c_g^m)] \quad (\text{A3})$$

where $\Delta h_v^m = -k_B T \ln c_{ve}^m$, $\Delta h_g^m = -k_B T \ln c_{ge}^m$, and $\Delta h_m^m = -k_B T \ln(1-c_{ve}^m-c_{ge}^m)$ are the formation energy of a vacancy, a gas atom, and an UO_2 molecule in the matrix, respectively.

The chemical free energy density in the matrix is

$$\begin{aligned} f^m &= H^m - TS^m \\ &= k_B T \left[c_v^m \ln \frac{c_v^m}{c_{ve}^m} + c_g^m \ln \frac{c_g^m}{c_{ge}^m} + (1-c_v^m-c_g^m) \ln \frac{1-c_v^m-c_g^m}{1-c_{ve}^m-c_{ge}^m} \right] \end{aligned} \quad (\text{A4})$$

Derivation of chemical free energy density of the gas bubble

We consider a bubble consisting of n lattice sites that has n_v vacancies and $n-n_v$ UO_2 particles. Thus, there are $n_v!/[n_v!(n-n_v)!]$ microstates due to the vacancy distribution. Because Xe gas atoms can only be located at vacancy lattice sites, there are $n_{gm}!/[n_g!(n_{gm}-n_g)!]$ microstates due to the distribution of n_g Xe gas atoms in the space consisting of n_v vacancies that can hold a maximum of n_{gm} Xe gas atoms. $n_{gm}b = n_v\Omega$, $n_{gm} = n_v\Omega/b$, where Ω is the volume of a vacancy and b the volume of a Xe gas atom. Therefore, there are w^b microstates in the bubble

$$w^b = \frac{n!}{n_v!(n-n_v)!} \frac{n_{gm}!}{n_g!(n_{gm}-n_g)!} \quad (\text{A6})$$

The entropy of the above distribution is

$$\begin{aligned} s^b &= k_B \ln w^b = k_B \ln \frac{n!}{n_v!(n-n_v)!} \frac{n_{gm}!}{n_g!(n_{gm}-n_g)!} \\ &\approx -nk_B [c_v^b \ln c_v^b + (1-c_v^b) \ln(1-c_v^b) + c_{gm} \ln c_{gm} - c_g^b \ln c_g^b - (c_{gm}-c_g^b) \ln(c_{gm}-c_g^b)] \end{aligned} \quad (\text{A7})$$

where $c_v^b = n_v/n$, $c_g^b = n_g/n$ and $c_{gm} = n_{gm}/n = \Omega/b$.

In the phase-field method, a bubble or void is treated as a phase, and UO_2 vacancies are considered as a kind of particle. With only the linear terms remaining, the enthalpy due to the interaction between UO_2 particles and UO_2 vacancies is $\Delta h_v^b n_v + \Delta h_m^b n_m$, and that due to the interaction between UO_2 vacancies and Xe gas atoms is $\Delta h_{vv}^b n_{vv} + \Delta h_g^b n_g$. The number of vacancy sites that are not occupied by gas atom is $n_{vv} = n_{gm} - n_g$. The enthalpy in the bubble is written as follows

$$\begin{aligned} H^b &= \Delta h_v^b n_v + \Delta h_m^b n_m + \Delta h_{vv}^b n_{vv} + \Delta h_g^b n_g \\ &= \Delta h_v^b n_v + \Delta h_m^b (n-n_v) + \Delta h_{vv}^b (n_{gm}-n_g) + \Delta h_g^b n_g \\ &= n [\Delta h_v^b c_v^b + \Delta h_m^b (1-c_v^b) + \Delta h_{vv}^b (c_{gm}-c_g^b) + \Delta h_g^b c_g^b] \end{aligned} \quad (\text{A8})$$

where $\Delta h_v^b = -k_B T \ln c_{ve}^b$, $\Delta h_m^b = -k_B T \ln(1-c_{ve}^b)$, $\Delta h_{vv}^b = -k_B T \ln(c_{gm}-c_{ge}^b)$ and $\Delta h_g^b = -k_B T \ln c_{ge}^b$. Thus, the chemical free energy density in the bubble is

$$\begin{aligned} f^b &= H^b - TS^b \\ &= k_B T \left[c_v^b \ln \frac{c_v^b}{c_{ve}^b} + (1-c_v^b) \ln \frac{1-c_v^b}{1-c_{ve}^b} + c_g^b \ln \frac{c_g^b}{c_{ge}^b} + (c_{gm}-c_g^b) \ln \frac{c_{gm}-c_g^b}{c_{gm}-c_{ge}^b} \right] \end{aligned} \quad (\text{A9})$$

Appendix B

At very high pressures, the Van der Waals equation is written as:

$$P_g = k_B T / (v - b) \quad (\text{B1})$$

where b is the Van der Waals constant, which accounts for the repulsive component of the interatomic potential. Due to the high gas atom density

in the bubble, the other constant in the Van der Waals equation that reflects the attractive portion of the potential is neglected. k_B is the Boltzmann constant, T is the absolute temperature, and v is the volume occupied by one Xe gas atom in a bubble with radius r .

$$v = 4\pi r^3/3n_g \quad (\text{B2})$$

where n_g is the number of Xe gas atoms in the bubble. Substituting the above expression into expression (B1), we get

$$P_g = \frac{3n_g k_B T}{4\pi r^3 - 3bn_g} \quad (\text{B3})$$

or

$$n_g = \frac{4\pi r^3 P_g}{3(k_B T + P_g b)} \quad (\text{B4})$$

There are m vacancies in the bubble.

$$m = 4\pi r^3/3\Omega \quad (\text{B5})$$

Ω is the volume of one molecule of UO_2 . Therefore, we can get the expression of equilibrium gas atom concentration in a bubble

$$c_{ge}^b = \frac{n_g}{m} = \frac{P_g \Omega}{k_B T + P_g b} \quad (\text{B6})$$

For the bubble surface under the mechanical equilibrium condition, the following relation exists:

$$P_g + \sigma_{bk} = \frac{2\gamma_s}{R} \quad (\text{B7})$$

where σ_{bk} is the stress in the bulk, R is the bubble radius, and γ_s is the surface tension of UO_2 . Under stress-free conditions, $\sigma_{bk} = 0$, one can obtain the pressure in the bubble, which can be rewritten as follows:

$$P_{ge} = 2\gamma_s/R \quad (\text{B8})$$

This is a function of the surface tension and the radius of the bubble. Thus, under stress-free conditions, the equilibrium gas atom concentration in a bubble can be written as follows:

$$c_{ge}^b = \frac{\Omega}{Rk_B T/2\gamma_s + b} \quad (\text{B9})$$

References

- [1] I. Zacharie, S. Lansiaert, P. Combette, M. Trotabas, M. Coster, M. Groos, J. Nucl. Mater. 255 (1998) 85–91.
- [2] P. Garcia, G. Martin, C. Sabathier, G. Carlot, A. Michel, P. Martin, B. Dorado, M. Freyss, M. Bertolus, R. Skorek, J. Noirot, L. Noirot, O. Kaitasov, S. Maillard, Nuclear Instruments and Methods in Physics Research Section B: Beam Interactions with Materials and Atoms, 277 (2012) 98–108.
- [3] R. Bès, P. Martin, E. Vathonne, R. Delorme, C. Sabathier, M. Freyss, M. Bertolus, P. Glatzel, Appl. Phys. Lett. 106 (2015) 114102.
- [4] P.M. Martin, E. Vathonne, G. Carlot, R. Delorme, C. Sabathier, M. Freyss, P. Garcia, M. Bertolus, P. Glatzel, O. Proux, J. Nucl. Mater. 466 (2015) 379–392.
- [5] S.T. Murphy, A. Chartier, L. Van Brutzel, J.P. Crocombette, Physical Review B 85 (2012).
- [6] R. Jackson, C. Catlow, J. Nucl. Mater. 127 (1985) 161–166.
- [7] C. Sabathier, L. Vincent, P. Garcia, F. Garrido, G. Carlot, L. Thome, P. Martin, C. Valot, Nucl. Instrum. Methods Phys. Res., Sect. B 266 (2008) 3027–3032.
- [8] L. Liang, Y.S. Kim, Z.-G. Mei, L.K. Aagesen, A.M. Yacout, J. Nucl. Mater. 511 (2018) 438–445.
- [9] W. Chen, X.-M. Bai, Jom, (2020).
- [10] S.R. Phillpot, A. El-Azab, A. Chernatynskiy, J.S. Tulenko, Jom 63 (2011) 73.
- [11] C.T. Walker, D. Staicu, M. Sheindlin, D. Papaioannou, W. Goll, F. Sontheimer, J. Nucl. Mater. 350 (2006) 19–39.
- [12] J.K. Fink, J. Nucl. Mater. 279 (2000) 1–18.
- [13] W. Oldfield, J. Brown, Materials Science and Engineering 6 (1970) 361–370.
- [14] J. MacEwan, V. Lawson, J. Am. Ceram. Soc. 45 (1962) 42–46.
- [15] C. Olsen, in, Idaho National Engineering Lab., Idaho Falls (USA), 1979.
- [16] F. Nichols, J. Nucl. Mater. 84 (1979) 319–326.
- [17] B. Marchand, N. Moncoffre, Y. Pipon, N. Béreard, C. Garnier, L. Raimbault, P. Sainsot, T. Epicier, C. Delafoy, M. Fraczkiewicz, C. Gaillard, N. Toulhoat, A. Perrat-Mabilon, C. Peaucelle, J. Nucl. Mater. 440 (2013) 562–567.
- [18] B. Marchand, N. Moncoffre, Y. Pipon, C. Garnier, N. Béreard, C. Delafoy, M. Fraczkiewicz, A. Perrat-Mabilon, L. Raimbault, P. Sainsot, N. Toulhoat, Prog. Nucl. Energy 57 (2012) 145–149.
- [19] H. Kawamata, H. Kaneko, H. Furuya, M. Koizumi, J. Nucl. Mater. 68 (1977) 48–53.
- [20] J.K. Platten, J. Appl. Mech. 73 (2006) 5–15.
- [21] R. Barnes, D. Mazey, Proc. R. Soc. Lond. A 275 (1963) 47–57.
- [22] M. Speight, J. Nucl. Mater. 13 (1964) 207–209.
- [23] P. Sens, J. Nucl. Mater. 43 (1972) 293–307.
- [24] V. Tikare, E.A. Holm, J. Am. Ceram. Soc. 81 (1998) 480–484.
- [25] T.G. Desai, P. Millett, M. Tonks, D. Wolf, Acta Mater. 58 (2010) 330–339.
- [26] L. Zhang, M.R. Tonks, P.C. Millett, Y. Zhang, K. Chockalingam, B. Biner, Comput. Mater. Sci. 56 (2012) 161–165.
- [27] I.W. Vance, P.C. Millett, J. Nucl. Mater. 490 (2017) 299–304.
- [28] S.Y. Hu, C.H. Henager Jr, Acta Mater. 58 (2010) 3230–3237.
- [29] Y. Li, S. Hu, X. Sun, F. Gao, C.H. Henager, M. Khaleel, J. Nucl. Mater. 407 (2010) 119–125.
- [30] S. Novascone, P. Medvedev, J.W. Peterson, Y. Zhang, J. Hales, J. Nucl. Mater. 508 (2018) 226–236.
- [31] Y. Li, S. Hu, X. Sun, M. Stan, npj Computational Materials, 3 (2017).
- [32] L.K. Aagesen, D. Schwen, M.R. Tonks, Y. Zhang, Comput. Mater. Sci. 161 (2019) 35–45.
- [33] M.R. Tonks, A. Cheniour, L. Aagesen, Comput. Mater. Sci. 147 (2018) 353–362.
- [34] D. Olander, Fundamental Aspects of Nuclear Reactor Fuel Elements, Us Dept of Energy, 1976.
- [35] F. Nichols, Acta Metall. 20 (1972) 207–214.
- [36] F. Nichols, J. Nucl. Mater. 30 (1969) 143–165.
- [37] S.G. Kim, W.T. Kim, T. Suzuki, Phys. Rev. E 60 (1999) 7186.
- [38] R. Hall, M. Mortimer, D. Mortimer, J. Nucl. Mater. 148 (1987) 237–256.
- [39] K. Nogita, K. Une, Nucl. Instrum. Methods Phys. Res., Sect. B 141 (1998) 481–486.
- [40] J.W. Cahn, J.E. Hilliard, J. Chem. Phys. 28 (1958) 258–267.
- [41] Z. Xiao, M. Hao, X. Guo, G. Tang, S.-Q. Shi, J. Nucl. Mater. 459 (2015) 330–338.
- [42] J.W. Cahn, Acta Metall. 9 (1961) 795–801.
- [43] P.C. Millett, A. El-Azab, D. Wolf, Comput. Mater. Sci. 50 (2011) 960–970.
- [44] X. Ding, J. Zhao, H. Huang, S. Ding, Y. Huo, J. Nucl. Mater. 480 (2016) 120–128.
- [45] F. Nichols, J. Nucl. Mater. 22 (1967) 214–222.
- [46] Y. Yun, H. Kim, H. Kim, K. Park, J. Nucl. Mater. 378 (2008) 40–44.
- [47] H. Matzke, J. Chem. Soc., Faraday Trans. 2 83 (1987) 1121–1142.
- [48] A. Whapham, Nucl. App. 2 (1966) 123–130.
- [49] C. Baker, J. Nucl. Mater. 71 (1977) 117–123.